

Bayesian graph convolutional neural networks via tempered MCMC

Rohitash Chandra^{1,**}, Ayush Bhagat^{2,**}, Manavendra Maharana², Pavel N. Krivitsky¹

Abstract

Deep learning models, such as convolutional neural networks, have long been applied to image and multi-media tasks, particularly those with structured data. More recently, there has been more attention to unstructured data that can be represented via graphs. These types of data are often found in health and medicine, social networks, and research data repositories. Graph convolutional neural networks have recently gained attention in the field of deep learning that takes advantage of graph-based data representation with automatic feature extraction via convolutions. Given popularity of these methods in a wide range of applications, robust uncertainty quantification is vital. This remains a challenge for large models and unstructured datasets. Bayesian inference provides a principled and robust approach to uncertainty quantification of model parameters for deep learning models. Although Bayesian inference has been used extensively elsewhere, its application to deep learning remains limited due to the computational requirements of the Markov Chain Monte Carlo (MCMC) methods. Recent advances in parallel computing and advanced proposal schemes in sampling, such as incorporating gradients has allowed Bayesian deep learning methods to be implemented. In this paper, we present Bayesian graph deep learning techniques that employ state-of-art methods such as tempered MCMC sampling and advanced proposal schemes. Our results show that Bayesian graph convolutional methods can provide accuracy similar to advanced learning methods while providing a better alternative for robust uncertainty quantification for key benchmark problems.

Keywords:

Bayesian neural networks, MCMC, Langevin Dynamics, Graph neural networks

1. Introduction

Graph neural networks are a type of artificial neural network designed for data which features graph-based representation [1, 2, 3, 4]. Graph-based representation can be used to analyse non-structured and non-sequential data, such as a social network comprising users and their activities [5]. Recently, a wide variety of graph-based deep learning network architectures has been introduced [3], such as graph convolutional neural networks (CNNs) [6, 7, 8], graph recurrent neural networks featuring long short-term memory (LSTM) networks [9, 10, 11, 12], graph auto-encoders [13, 14], and graph generative adversarial networks (GANs) [15]. Applications of graph neural networks have included time series forecasting [16], traffic flow forecasting [17, 18], particle physics [19], molecular property prediction [20], sentiment analysis [21], recommender systems [22], and social media popularity prediction [23]. We refer the reader to [24] for a further overview.

Deep learning methods, such as convolution neural networks [25, 26] (CNNs) and recurrent neural networks [27, 28] (RNNs) have been applied to image data and temporal sequences, but these are structured, regular, Euclidean data, though even they

can be viewed as graphs (i.e., lattices). CNNs and RNNs are less applicable to unstructured or graph-based data with multi-layer hierarchical structure, with features that occur on different scales.

On the other hand, graph neural networks (GNNs) use graph-based representation of data to propagate on each node. Aspects of the data such as the input order of the nodes are irrelevant, with the graph instead representing the dependencies between them; hence, GNNs can enable propagation guided by graph structure as done in canonical neural networks [29, 30].

As the impact of graph neural networks on different deep learning architectures and applications grows, there is also a growing need for robust uncertainty quantification in model parameters. Bayesian inference provides a means for robust uncertainty quantification in deep learning models by sampling from the posterior distribution that represents the model parameters [31, 32] using Markov-Chain Monte Carlo (MCMC) methods [33, 34]. This has proven challenging, however, given the size of the data and the number of model parameters in the models in question. MCMC methods have extensive computational requirements as thousands or samples needed for training, and so not much work has been done in implementing Bayesian CNNs via MCMC sampling. Variational inference, provides an alternative for uncertainty quantification in deep learning methods via Bayes by backpropagation [35]. At the same time, there has been progress in the MCMC approach, making use of parallel computing and advanced MCMC methods [33, 34], which may enable the framework to be applied to graph CNNs. Advanced proposal distribution in MCMC that

*Corresponding author

**Equal contributions

Email address: rohitash.chandra@unsw.edu.au (Rohitash Chandra)

¹School of Mathematics and Statistics, UNSW Sydney, Kensington, NSW 2052, Australia

²Manipal Institute of Technology, India

incorporate gradients [36, 32] has opened the door to Bayesian deep learning methods for novel deep learning methods.

In this paper, we present a Bayesian graph deep learning approach that employs state-of-art methods, such as tempered MCMC sampling and sophisticated advanced proposal schemes. We then apply our methods to selected benchmark graph-based datasets obtained from research data repositories such as *PubMed*³. We use parallel computing framework where MCMC samplers are executed in parallel with interprocess communication demonstrated in our previous work [36] for sampling weights and biases of the graph CNN model.

The remainder of the paper is organised as follows. In Section 2, we review the background of the problem and related methods. Section 3 presents the proposed methodology, followed by experiments and results in Section 4. We discuss the implications of our work and directions of future work in Section 5, and Section 6 concludes the paper.

2. Background and Related Work

2.1. Graph neural networks

A graph G data structure consists of a set of vertices (nodes) V and edges E , which can be either directed or undirected [37, 38]. Each node represents a data element, and the edges denote the relationships between the data elements. Each node has its own graph embedding via a feature vector, which summarises the properties of that particular data element. The nodes send their graph embedding to their immediate neighbours in the form of messages [39].

The message received by node v at time t , m_v^t is constructed by aggregating over the set of neighbours v , $N(v)$, the results of a message function M_t which takes three arguments: the feature vector of v itself (h_v^t), the feature vector of neighbour w (h_w^t), and the features of the edge between v and w (e_{vw}):

$$m_v^t = \sum_{w \in N(v)} M_t(h_v^t, h_w^t, e_{vw}).$$

Based on this message m_v^t and the previous value h_v^t , the latter is updated via a function U_t :

$$h_v^{t+1} = U_t(h_v^t, m_v^t).$$

A variety of graph representations are possible, including directed graphs, heterogeneous graphs, edge information graphs, and dynamic graphs [24]. The goal of GNN is to learn a state embedding which incorporates the neighbourhood information of for each node; this state embedding can then be used for classification and other purposes. The choice of the propagation and the output step of a GNN are required to obtain the hidden states of nodes or edges and depend on the application. In relation to the canonical GNNs, the focus has been on refinements in the propagation step, while a simple feedforward neural network is retained in the output step. The major variants in the propagation step utilise different aggregators to gather information from each node’s neighbors. Some

of the key propagation step methods include attention aggregator (graph attention network [40] and gated attention network [41]), gated aggregator (gated graph neural networks [42] and graph LSTM [43]), skip connection (highway GNN [44] and jump-knowledge network [45]), hierarchical graph edge conditioned convolution [46]), and finally convolutional aggregator, which features graph CNN with spatial [47] and spectral methods [30]. Spatial methods in graph CNNs include Neural Fingerprints (FPs) [48], dual graph convolution network (DGCN) [49], and model networks (MoNet) [50]. Some of the commonly used spectral methods in graph CNNs are ChebNet (Chebyshev polynomial approximation algorithm) [51], GCN (Graph Convolutional Network is first-order approximation of graph convolutions) [30], and adaptive graph convolutional networks (AGCN) [52]. In spectral convolution, the underlying structure of the graph is deduced by eigendecomposition of the graph Laplacian. The entire graph is processed simultaneously, which makes spectral convolution more computationally expensive. However, it is still widely used, because the spectral filters excel at capturing complex patterns. Spatial methods use information from neighbouring nodes and deduce properties of a node based on features of its closest k neighbours. The graph can be processed in batches of nodes, which help improve speed and efficiency.

A number of approaches can be used to update or training GNNs. They include neighbourhood sampling (Graph SAGE [53], PinSage [54] and FastGCN [55]), receptive field control [56], data augmentation such as co-training [57] and self-training [57], and unsupervised training such as Graph Autoencoder (GAE) [58] and Adversarially Regularized Graph Autoencoder (ARGA) [59].

2.2. Bayesian deep learning

Research in area of Bayesian deep learning has been limited due to the limitations of canonical MCMC methods for large number of parameters, characteristic of deep learning models [60, 61]. As we noted earlier, variational inference provides a computationally cheaper approach, with variational autoencoders [62], variational autoencoders and GANs [63], pruned variational CNNs [64, 65, 66], variational RNNs and long short-term memory (LSTM) networks [67], recurrent variational graph convolutions [68], and variational graph neural networks with focus on autoencoders [58] and Markov networks [69]. Most of these methods were developed in the last five years, particularly after 2017, with applications summarised in [60]. Although work has been done in area of variational CNNs [70], we did not find any work in the area of variational graph-CNNs.

Over the last decade, with improving computational resources and advanced MCMC strategies, advanced proposal distributions incorporating gradients have been applied, with Langevin and Hamiltonian MCMC [32, 71]. However, only in last five years has there been progress in area of Bayesian neural networks with Hamiltonian MCMC [72], and graphic processing unit (GPU) implementation to enhance computation [73]. Recent work in area where Langevin MCMC methods have been used for neural networks include the use of parallel tempering MCMC for simple neural networks for pattern classifica-

³<https://pubmed.ncbi.nlm.nih.gov/>

tion and time series prediction problems [36]. There has also been some progress in the use of surrogate assisted estimation for Bayesian neural networks given that the model and data are computationally expensive or difficult to sample [74] and incorporating transfer learning to take advantage of multiple sources of data in a Bayesian framework via Langevin MCMC sampling [75]. Although simple neural networks have been used in pattern classification problems [74, 75], some of the problems have had large numbers of features, and hence the neural network models had more than 5,000 parameters, comparable to smaller deep learning models.

3. Methodology

In this section, we present details for Bayesian graph convolutional neural networks (Bayes-GCNN), which uses spectral convolution and parallel tempering MCMC sampling framework with Langevin-gradient proposal distribution for classification of nodes in datasets with graph representation.

3.1. Model and likelihood function

In conventional CNNs, the input data are multiplied by a matrix of weights having the same dimension as the input data. This matrix of weights is known as the *filter* or *kernel*. A single layer can have multiple filters to extract different features in the data. The output can then be fed into more convolution layers or pooling layers to extract the prominent features of the data. Given a CNN with multiple layers, the output Y_i^l for layer l with m_l filters is computed as follows

$$Y_i^{(l)} = B_i^{(l)} + \sum_{j=1}^{m_l^{(l-1)}} K_{i,j}^{(l)} X_i^{(l-1)} \quad (1)$$

where, $B_i^{(l)}$ is the bias matrix, $X_i^{(l-1)}$ is the input data to the layer and $K_{i,j}^{(l)}$ is the filter.

In comparison to conventional neural networks, graph neural networks do not operate on euclidean data, with a fixed dimension and a tabular structure. Graph information such as the edge directionality, node attributes, and edge attributes cannot necessarily be mapped to a higher dimension euclidean space. In our proposed Bayesian graph CNN (Bayes-GCNN), we use the fast approximate spectral graph convolution technique of Kipf et al. [30] instead. We adapt (1) such that it can work on graphs, where the number of node connections is dynamic and the nodes are unordered. Kipf et al. gives us the equation to compute the convolved signal matrix as follows

$$Z = D^{(-1/2)} A D^{(-1/2)} X \theta$$

where Z is the convolved signal matrix, D is the degree matrix, A is the adjacency matrix, X is the node feature vector and θ is a matrix of filter parameters.

Our focus in this paper will be application of Bayes-CNN to node classification using graph datasets, and so we construct the likelihood function that will be used for MCMC sampling of parameters (weights and biases) in Bayes-GCNN. The likelihood

function enables the comparison of the training data featuring graph representation \mathbf{x} with graph CNN output $\mathbf{x}' = z(\mathbf{x}, w, b)$, where w and b are the Bayes-GCNN parameters (weights and biases combined) shown in Figure 1, respectively. These weights and biases include those in convolution and max-pooling layers of graph CNN.

Pattern classification problems entail discrete outcomes, and thus we use a multinomial likelihood function. Suppose that we have K classes in the training data, and assume that the dataset $\mathbf{x} = (x_1, \dots, x_N)$ is drawn from a multinomial distribution with parameters $\theta = (\theta_1, \dots, \theta_K)$, for $\sum_{k=1}^K \theta_k = 1$. Define indicator variables

$$z_{i,k} = \begin{cases} 1, & \text{if } x_i = k \\ 0, & \text{otherwise} \end{cases}$$

for observations $i = 1, \dots, N$ and classes $k = 1, \dots, K$. Then, the multinomial likelihood function can be expressed

$$p(\mathbf{x}|\theta) = \prod_{i=1}^N \prod_{k=1}^K \theta_{i,k}^{z_{i,k}}, \quad (2)$$

where $\theta_{i,k}$ is the Bayes-GCNN model's predicted probability that observation i is in class k . We use a multinomial expit function to link the output of the Bayes-GCNN model $f_{(i)}$ (for input features x_i) to the predicted probability:

$$\theta_{i,k} = \frac{\exp(f_k(x_i))}{\sum_{j=1}^K \exp(f_j(x_i))}.$$

The prior distribution is given by

$$p(\theta) \propto \frac{1}{(2\pi\sigma^2)^{P/2}} \times \exp\left\{-\frac{1}{2\sigma^2}\left(\sum_{i=1}^P \theta_i^2\right)\right\} \quad (3)$$

where θ represents the GCNN parameters (weights and biases), P is the total number of parameters, and σ^2 is user-defined variance, typically obtained from prior knowledge about distribution of parameters in trained neural networks.

Our implementation performs these calculations on the log scale to minimise numerical instability.

3.2. Langevin-gradient proposal distribution

Next, we use MCMC sampling to sample the posterior distribution of weights and biases of Bayes-GCNN. For deep learning models (graph-based CNNs), that can feature hundreds of thousands of parameters, state-of-art MCMC sampling methods are needed. Therefore, we employ 1) efficient proposal distribution via Langevin-gradients, 2) parallel computing that features inter-process communication, and 3) parallel tempering MCMC to optimise sampling from multi-modal posterior distributions.

The Langevin-gradient proposal distribution essentially incorporates Gaussian noise with a gradient step taken using a single iteration (epoch) [32]. The gradient step can be either in form of stochastic-gradient descent (SGD) or adaptive gradient-descent, such as the Adam optimiser [76, 36]. At a given step or chain position (n) of a MCMC sampler, we create a proposal

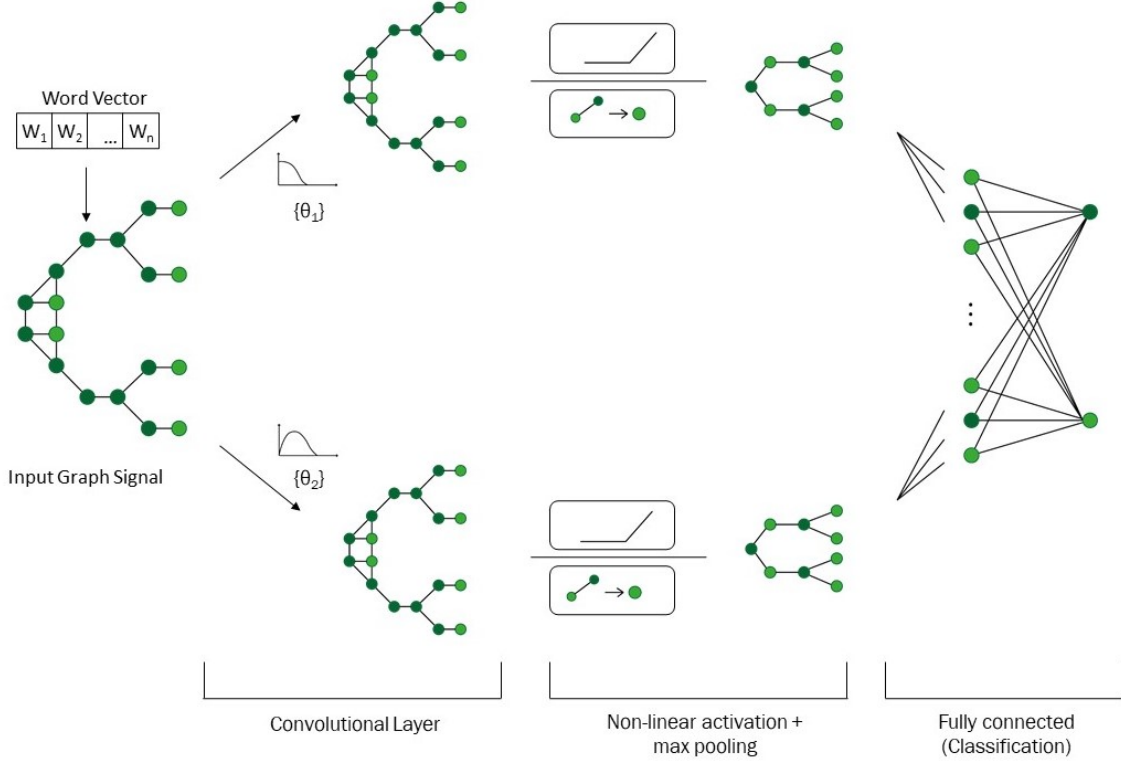


Figure 1: Graph CNN

denoted by superscript (\star) from a multivariate normal distribution θ_n^\star as follows:

$$\theta_n^\star \sim \mathcal{N}(\theta_n + \nu_1 \bar{v}_n, \nu_2^2 I_P). \quad (4)$$

Here, I_P is an $P \times P$ identity matrix, scaled by the tuning parameter ν_2^2 ; and \bar{v}_n is the Langevin gradient $\nabla_\theta \log\{p(\theta)p(\mathbf{x}|\theta)\}$ (3) and (2), respectively, scaled by ν_1 , either fixed in the case of stochastic-gradient-descent-based algorithm or adaptive in the case of an Adam-based algorithm [76]. Thus, the proposal attempts to “climb” up the posterior density. The Metropolis–Hastings probability (α) is used to accept/reject a proposed sample is as follow:

$$\alpha = \min \left\{ 1, \frac{p(\mathbf{x}|\theta_n^\star)p(\theta_n^\star)Q(\theta_n|\theta_n^\star)}{p(\mathbf{x}|\theta_n)p(\theta_n)Q(\theta_n^\star|\theta_n)} \right\},$$

where $Q(\theta_n^\star|\theta_n) = p(\theta_n^\star|\theta_n)$, the conditional proposal density and vice versa. Calculating the Q ratio is necessary because the Langevin-gradients are not symmetric at different steps in the chain when.

3.3. MCMC Sampling

Initially motivated by thermodynamics, *Parallel tempering MCMC (tempered, replica exchange)* MCMC [77, 78, 79, 77], samples an ensemble of M MCMC replicas $\Omega = [R_1, R_2, \dots, R_M]$ each with a different temperature, $T = [1, \dots, T_{\max}]$, typically geometrically spaced, with T_{\max} defined by the user to control the extent of exploration. The likelihood of each replica in the ensemble is attenuated to form a n attenuated posterior distribution $p_t(\theta_n^t|\mathbf{x}) \propto p(\mathbf{x}|\theta_n^t)^{1/t} p(\theta_n^t)$. This “flattens” the distribution,

increasing the Metropolis–Hastings acceptance rates for higher t , which also helps in escaping from local minima. The neighbouring replicas are periodically exchanged via a Metropolis–Hastings step, balancing exploration and exploitation [80, 81].

Effectively, this augments the sample space of θ_n into $\theta_n^t = (\theta, \tau^2, t)$, sampling jointly across θ and t . Those realisations with $t = 1$ then have the target distribution. Therefore, periodically, a proposal is made to exchange the states of the neighbouring replicas, so that $\theta_n^t = \theta_n^{t+1}$ and $\theta_n^{t+1} = \theta_n^t$. This proposal is symmetric, and the priors cancel, so the acceptance probability

$$\beta = \min \left\{ 1, \frac{P(\mathbf{x}|\theta_n^t)^{1/(t+1)} P(\mathbf{x}|\theta_n^{t+1})^{1/t}}{P(\mathbf{x}|\theta_n^{t+1})^{1/(t+1)} P(\mathbf{x}|\theta_n^t)^{1/t}} \right\}.$$

Our parallel tempering MCMC framework for Bayes-GCNN employs parallel processing cores for execution of MCMC replicas that exchange states at regular interval via inter-process communication. The Bayes-GCNN framework that features parallel MCMC replica samplers, inter-process communication, and graph-based data is shown in Figure 2, and presented in Algorithm 1. We begin by defining the graph-CNN architecture that includes the size of convolution and max-pooling layers and number of output neurons given by the classification problem with given graph-based data representation for input as shown in Figure 1.

3.4. Combined Algorithm

The combined algorithm requires some tuning. In addition to the configuration of the neural network, the user sets the

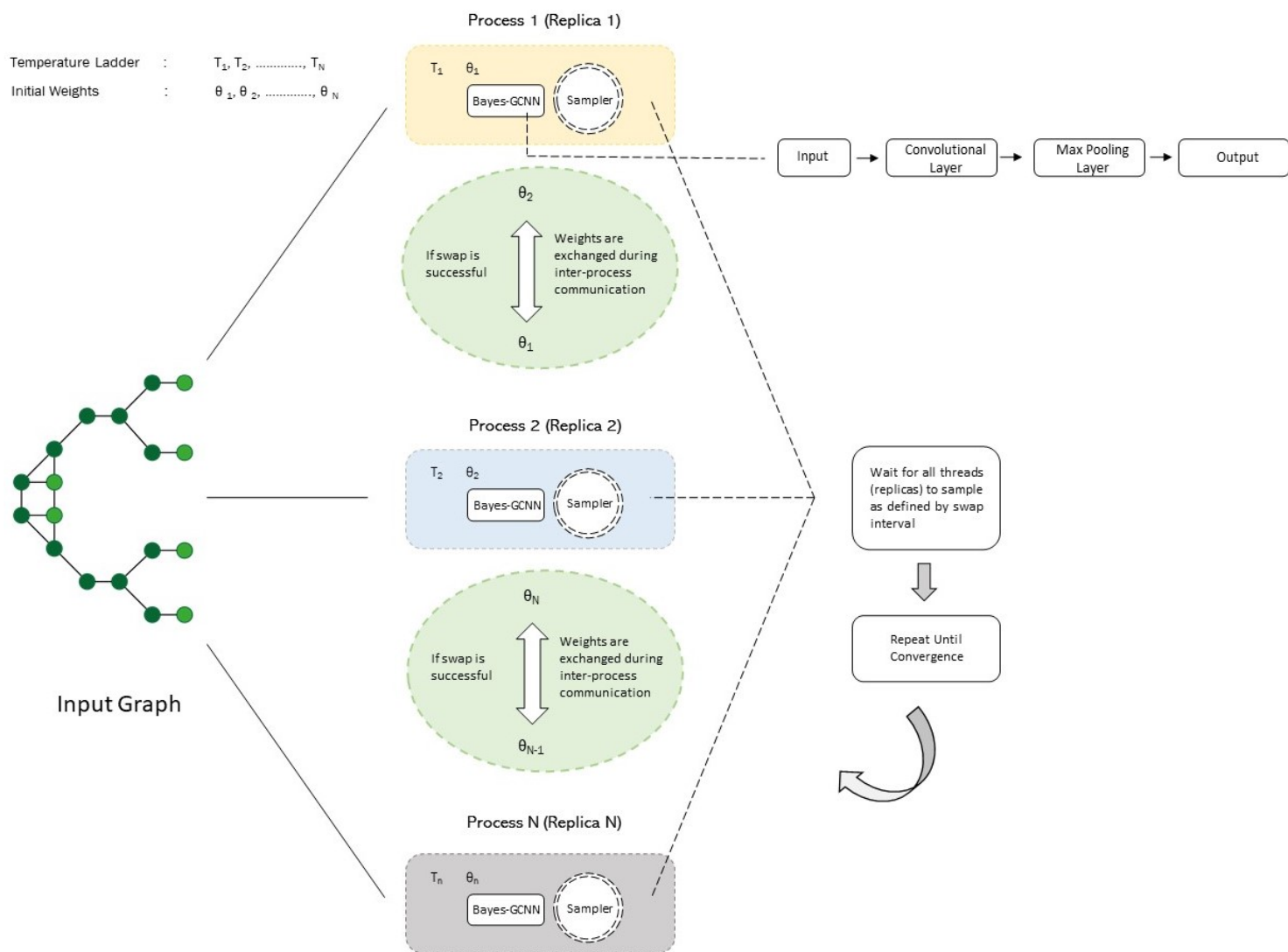


Figure 2: Bayesian CNN framework highlighting tempered MCMC utilising parallel computing and CNN.

number of replicas (M), maximum temperature of the temperature ladder (T_{\max}), neighbouring replica swap-interval (R_{swap}), and maximum number of replica samples (R_{\max}). The user must also set the Langevin-gradient rate, l_{rate} determines how often it is used for creating the proposal, as opposed to a random-walk proposal (effectively setting $v_1 = 0$).

Parallel tempering MCMC is used in first-phase of Algorithm 1, then it switches to canonical MCMC in second-phase defined by R_{switch} to further balance global exploration with local and to ensure that the true posterior distribution is sampled during the end. When R_{switch} is reached, the respective replica temperature is changed to 1 as done in our previous works [36, 82]. Our implementation tracks the number of “active” (tempered) replicas in the ensemble, starting with $active = M$ and decrementing it as replicas turn into canonical MCMC.

In Algorithm 1, the execution begins with parallel tempering replica sampling (Stage 1.1) with the manager process overseeing parallel replica processes. Each replica sample creates a proposal depending on the l_{rate} (Stage 1.2) using either random-walk or Langevin-gradients (4). In Stage 1.3, the log-likelihood is computed along with the Metropolis–Hastings probability (Stage 1.4) to accept/reject a proposed sample. Then, the algorithm checks (Stage 1.5) whether to carry on with parallel tempering MCMC or change the replica temperature values to 1 for canonical MCMC. Next the replica exchange is done depending on the replica swap-interval (R_{swap}) and Metropolis–Hastings probability (Stage 2.2) which considers the log-likelihood of neighboring replica processes. We note that the manager process is used to determine if the neighboring replicas can be swapped. In case if they are swapped, the chain position is exchanged via inter-process communication. Finally, the algorithm decrements the number of active replicas if the maximum number of replica samples (R_{\max}) are reached which enables the algorithm to end replica sampling. In post-replica sample stage (Stage 4), burn-in sampling period is removed (which includes first sage sampling by parallel tempering MCMC) and then combined with respective replica posterior distribution of Bayes-GCNN for further analysis. In this way, parallel tempering is used for exploration but the samples do not become part of the true posterior, since it has pseudo-posterior distribution (due to the temperature level affecting the replica log-likelihood).

4. Experiments and Results

We evaluate distinct features of Bayesian graph convolutional neural networks (GCNNs) in terms of computational efficiency of parallel tempering MCMC sampling, effect of Langevin-gradient proposal distribution, and prediction accuracy for established benchmark datasets.

4.1. Dataset description

We use Cora [83], CiteSeer [84] and PubMed [85] citation network datasets, which are commonly used to evaluate graph neural networks. Each dataset is one connected graph consisting of nodes, each representing a scientific publication. The

Data: Graph-based Data

Result: Bayes-GCNN posterior distribution

Stage 0: initialisation:

* Define Baye-GCNN architecture (number of input, convolution and pooling layers, number of outputs, and respective activation functions). * Provide user-defined parameters: maximum temperature (T_{\max}), swap-interval (R_{swap}), and maximum replica samples (R_{\max}).

* Termination condition: Set $active = M$

* Define (R_{switch}) for parallel tempering MCMC to canonical MCMC

* Define l_{rate} for applying Langevin-gradients.

while ($alive \neq 0$) **do**

Stage 1.0: Execute each replica via manager process

for $i = 1$ **to** M **do**

$s = 0$

phase-one: $T_i = \text{geometric}()$

for $s = 1$ **to** R_{\max} **do**

Stage 1.1: Local Replica Sampling

for $k = 1$ **to** R_{swap} **do**

1.2 **if** $\text{Unif}(0, 1) \leq g_{\text{prob}}$ **then**
| Langevin-gradient proposal

else
| Random-walk proposal

end

1.3 Get log-likelihood and computer

Metropolis-Hastings probability α

1.4 **if** $\text{Unif}(0, 1) \leq \alpha$ **then**
| Accept proposal, $\theta_s \leftarrow \theta_s^*$

else
| Reject proposed sample, retain current
sample: $\theta_s \leftarrow \theta_{s-1}^*$

end

1.5 **if** phase-two is true **then**
| Change replica temperature, $T_i = 1$

end

end

Stage 2.0: Neighbouring replica exchange:

2.1 Get neighbouring replica Metropolis-Hastings acceptance probability β

2.2 **if** $\text{Unif}(0, 1) \leq \beta$ **then**

| Give signal() to the manager process Exchange replicas, $\theta_i \leftrightarrow \theta_{s+1}$

end

end

end

Stage 3.0: Signal() manager process

3.1 Decrement number of replica processes $alive$

end

Stage 4: Combine posterior using second-phase MCMC samples

Algorithm 1: Parallel tempering MCMC for Bayesian Graph Neural Networks. The manager process is highlighted in blue and replica processes running in parallel is highlighted in pink.

edges of the graph serve as citation links between the scientific publications (nodes). Each publication in each dataset is described by a word vector indicating the absence/presence of the corresponding word from the dictionary. The details of the dataset in terms of number of nodes, edges, classes and training and test samples are provided in Table 1. We note that number of training instances is relatively low; however, this specific data split is used in the literature [29] and we use it for uniformity in comparing results.

The Cora dataset consists of citation information for 2708 machine Learning papers with 1433 unique words in its dictionary. The nodes are classified into 7 labels: “case-based”, “genetic algorithms”, “neural networks”, “probabilistic methods”, “reinforcement learning”, “rule learning”, and “theory”. The CiteSeer dataset extracted from the CiteSeer digital library consists of 3327 scientific papers with 3703 unique words in its dictionary. The nodes are classified into 6 labels: “agents”, “artificial intelligence”, “DB”, “IR”, “machine learning”, “human computer interface”. The PubMed dataset features papers about diabetes which contains 19717 scientific papers and 44,338 citation links with 500 unique words in the dictionary. The nodes are classified into 3 classes which include “diabetes mellitus, experimental”, “diabetes mellitus Type 1” and “diabetes mellitus Type 2”.

4.2. Experiment Design

We first run a number of experiments to assess the effect parallel tempering tuning parameters. We benchmark performance, computational time, and classification accuracy. In the respective datasets, we use the data split used in previous work [29], which has 20 labels per class for training, and 1000 nodes for testing.

In all experiments, we use the following parallel tempering MCMC parameters determined in our experiments. In random-walk proposals, the Gaussian noise added is with standard deviation of $\nu_2 = 0.005$. We use maximum temperature ($T_{\max} = 2$), R_{switch} as 60% of total samples and swap interval $R_{\text{swap}} = 2$ samples (iterations) for all experiments. We tried using $M = 2, 4, 6, 8, 10$ replicas. In all the experiments, we use a maximum of 48,000 samples which are distributed across the given number of replica chains.

Bayes-GCNN is implemented using pyTorch⁴ and pyTorch-geometric libraries⁵ and Python multi-processing library for parallel MCMC replica processes. The topology of Bayes-GCNN in terms of number of input, hidden, and output neurons for each of the datasets is given in Table 2.

Our Langevin-gradients implementation can use either the using the Adam optimiser which uses first and second order moments of past gradients to adapt the learning rate ν_1 [76] or the standard Gradient Descent. An initial (seed) learning rate of 0.01 is used. This window includes the gradients of accepted and rejected samples during the MCMC sampling process. Past implementation of Langevin-gradients for Bayesian neural networks [36, 75, 74], stochastic gradient descent (SGD) was used

with user-chosen learning rate (i.e., constant ν_1). We provide comparison with SGD in the following section.

4.3. Results

We begin by evaluating the effect of Langevin-gradient (LG) proposal (as opposed to the random walk proposal) rate on the proposal distribution with 8 replicas in parallel tempering MCMC using the Cora dataset. Table 3 presents the classification accuracy on training and testing datasets (showing mean, best, and standard deviation), neighbouring replica swap rate (percentage), and percentage of accepted samples during sampling. We observe a positive association between the LG rate and percentage of acceptance samples which implies that LG provides better proposals when compared to random-walk proposal distribution. There is also an association between LG rate and computational time: computing gradients is expensive [36]. The accuracy for train and test dataset is much lower for LG rate of 0, which indicates that random-walk proposal distribution on its own cannot be used to train Bayesian GCNNs. However, higher Langevin rates do not appear to yield performance gains.

Table 4 shows the effect of number of replicas in parallel tempering MCMC for the Cora dataset according to the same metrics as above. We observe a reduction in computational time as the number of replicas increases from 2 to 4; however, the classification performance does not change much. This can be directly attributed to speed and efficiency gained by having more replica processes running in parallel (one replica process/thread per processing core). We also observe an increase in the swap percentage for up to 8 replicas, though a small one, in any case.

We then apply the Bayesian GCNN to the other datasets (CiteSeer and PubMed), using 8 replicas and LG rate of 0.75. The training and test classification accuracy that result are shown in Table 5. Prior literature does not always report the same summaries (best, mean, standard deviation) that we do, and so a direct comparison is not always possible; we compare the results assuming those from literature as the best performance unless otherwise indicated. In the case of GCNN (SGD) [29], we report the mean classification accuracy. We also show performance by our own implementation of canonical GCNN* using Adam and SGD learning algorithms with 30 experiential runs (mean, best and standard deviation) when compared with our proposed Bayes-GCNN. Note in case of Bayes-CNN, the mean, best and standard deviation are taken from posterior distribution of one experimental run.

Based on Table 5, our Bayes-GCNN (Adam) offers almost comparable – and even matching – performance if we compare the best classification accuracy for Bayes-GCNN (Adam) to those in the literature. Although Bayes-GCNN (Adam) offers slightly lower classification accuracy (taking account the mean performance), it provides comprehensive uncertainty quantification in predictions. We also note that using SGD rather than Adam for Langevin-gradients significantly reduces the performance of Bayes-GCNN, which is also the case of our canonical GCNN* model. The performance of GCNN (SGD) is significantly higher than that of canonical GCNN* (SGD) and Bayes-GCNN (SGD). This can be explained due to the difference in

⁴<https://pytorch.org/>

⁵<https://pytorch-geometric.readthedocs.io/en/latest/>

Table 1: Overview of datasets using graph representation showing number (num.) of classes with training, and test instances.

Dataset	Nodes	Edges	Num. classes	Num. training	Num. testing
Cora	2708	5429	7	140	1000
CiteSeer	3327	4732	6	120	1000
PubMed	19717	44338	3	60	1000

Table 2: Bayesian Graph Neural Network topology showing the total number of parameters (weights and biases).

Dataset	Input Neurons	Output Neurons	Hidden Layers	Total parameters
Cora	1433	7	16	23063
CiteSeer	3703	6	16	59366
PubMed	500	3	16	8067

Table 3: Effect of Langevin-gradient (LG) rate for MCMC sampling for Cora dataset.

LG Rate	Train Acc.(Mean, Max, Std)	Test Acc. (Mean, Max, Std)	Swap Per.	Accept Per.	Time (min.)
0	14.25 22.14 1.51	16.85 32.20 7.39	50.89	40.00	72.30
0.25	98.32 100.00 4.50	74.52 79.50 3.81	47.74	40.75	79.13
0.5	98.73 100.00 3.45	74.95 79.30 3.18	46.58	43.04	83.43
0.75	98.94 100.00 2.28	75.35 79.30 2.17	47.04	45.25	87.72
1.0	99.05 100.00 2.06	75.52 79.20 1.99	48.43	49.75	85.01

Table 4: Effect of number of replicas in parallel tempering MCMC for Cora dataset.

# Chains	Train Acc. (Mean, Max, Std)	Test Acc. (Mean, Max, Std)	Accept Per.	Swap Per.	Time (min.)
2	99.22 100.00 0.71	75.80 79.60 1.05	44.00	43.62	138.64
4	99.06 100.00 2.01	75.45 79.20 1.84	43.75	46.34	84.24
6	98.97 100.00 2.33	75.38 79.30 2.19	44.00	45.89	82.82
8	98.89 100.00 2.50	75.11 78.80 2.50	44.38	47.04	84.76
10	98.70 100.00 3.39	74.92 79.30 3.13	43.80	47.52	87.23

the method used for node classification. The canonical GCNN* (SGD) and Bayes-GCNN (SGD) use fast approximate convolutions as outlined in Kipf et al. [30], whereas the GCNN (SGD) uses an inductive method for semi-supervised learning on graph embedding. Hence, we can not make a direct comparison between the performance of SGD with respect to those models.

Figures 3–5 show the Bayes-GCNN trace plot and posterior distribution for selected parameters (weights) from the respective datasets. The trace plots show 8 replica samples with different colours post the burn-in period (hence all replica temperature values are 1). Figure 3 presents the results from the Cora dataset showing the trace-plots (Panels a and c) and the posterior distribution (Panels b and d) for two selected weights with evidence of a unimodal posterior distribution. This can be seen in the dense histograms having a single peak for both the weights (Panels b and d). In the case for the CiteSeer dataset shown in Figure 4, we get a similar observation where the selected weights are similar in trace plots (Panels a and c), and both the posterior distributions (Panels b and d) show a single peak and indicate a single node in a unimodal posterior. In Figure 5 (posterior for PubMed dataset), we see a striking contrast between the trace plots (Panels a and c) of the selected weights: the posterior distribution of the first weight (Panel b) indicates a unimodal posterior, and the posterior distribution of the second weight (Panel d) indicates a bimodal posterior. An explanation of this is that Cora and SiteSeer datasets employ a much larger

Bayes-GCNN given by the number of parameters when compared PubMed. (See Table 2.) All the trace plots show high correlation between the chains for all the respective datasets.

The reason behind the difference in the trace-plot and respective posterior distributions between the different datasets cant be explained without further analysis. We need to note that we are only selected two weights from thoughts of parameters and this is merely for visualisation of the sampling process and the investigation as to why we get unimodal or multimodal posterior for different datasets and Bayes-GCNN architectures is beyond the scope of the paper.

Figure 6 shows the log-likelihood plot along with the training and test classification accuracy for a single MCMC replica (with temperature level of 1) for the respective problems. In the respective problems (Panel a, b, and c), we observe that the log-likelihood value increases in value over the time (samples), leading to higher training and test classification accuracy. We also notice that the case of PubMed dataset in Panel c, is slightly different than Cora and CiteSeer datasets (Panel a and b). We find that PubMed dataset has a higher variance in test classification accuracy over time when compared to others. This could be purely due to the application problem and size of the datasets and the Bayes-GCNN architecture as shown in Table 2.

Next, we present results to verify if the Bayes-GCNN has converged using the Gelman–Reubin diagnostic [86]. Table 6 shows their values for selected weights for their respective prob-

lems; \hat{r} values close to 1 indicates convergence [86]. We use the different chain replicas for selected weights with unique identity number (Weight-ID) to determine if there is convergence between the MCMC replicas. The diagnostic uses the posterior distribution from all the replica chains after a burn-in of 60%. We observe that in Table 6, all the selected weight-IDs for the respective problems have values close to 1 and hence have obtained convergence.

5. Discussion

This paper serves as a proof of concept of implementing Bayesian inference via MCMC for GCNNs, achieving comparable performance (Table 5) with traditional methods, and provides a principled approach to uncertainty quantification for deep learning models.

We have observed that the Adam optimizer performed significantly better than SGD. This can be attributed to the fact that SGD maintains a single learning rate for all the weights whereas Adam maintains a separate learning rate for each weight and is adapted separately. This approach is better suited to make a large number of parameters converge than the traditional SGD optimiser. Since a single learning rate is used for all the weights in SGD, only a portion of the weights may reach their local minima; however, some of the weights may not converge leading to poor performance or inability to train as shown in Table 5 (Bayes-GNN (SGD)). In order to establish that Adam is better than SGD for Bayes-GCNNs, we would require more experimentation on datasets across different problem domains.

At the same time, the adaptive nature of Adam may also be a mild violation of the Markov assumption underpinning MCMC, since the exact step length depends on the prior 10 steps and the Q -ratio might be approximate; these requirements can be relaxed somewhat, but need to be checked carefully [87, for example], and doing so is subject for future work.

The Gelman–Rubin diagnostics has been the most commonly used method to evaluate convergence of Markov chains, due to ease of implementation and availability in software packages. However, it has also been reported to sometimes give a premature and unreliable convergence diagnosis, particularly in cases where the Markov chains are stuck in a local maxima [88]. Moreover, the effectiveness of Gelman–Rubin diagnostics for large numbers of parameters is not well been studied in the literature, and our model features tens of thousands. Hence, a better convergence diagnosis could be used to evaluate the Markov chains. Autocorrelation and effective sample size has also been widely used for MCMC convergence [89, 90], and their applicability for Bayesian deep learning models needs to also be evaluated.

The comparison of results with the literature motivates the implementation of Bayesian framework for other deep learning model, which includes LSTM and CNN models [48]. The uncertainty quantification in predictions can be useful for application areas, such as traffic forecasting [91] and emotion recognition [92]. We addressed graph-based CNNs in this paper, however, the approach can be used for other graph deep learning

architectures such as graph-LSTM networks [91, 92] and graph neural network [93].

The use of Bayesian MCMC schemes in graph neural networks is largely unexplored. Future work could focus on implementing Bayesian inference via MCMC for other architectures of graph Neural Networks, such as graph LSTM models [91] and graph attention networks [40] using different datasets such as Quantum Machine 9 (QM9) [94, 95], bioinformatics (enzymes) [96, 97], social news network (Reddit) [98]. Further work could also focus on the efficacy of other types of MCMC schemes such as Hamiltonian MCMC [99], in an attempt to further improve the classification accuracy performance.

6. Conclusion

We presented Bayes-GCNN, which takes advantage of parallel computing and an advanced MCMC scheme with efficient proposal distribution that takes into account gradients. Our results indicate that the method provides an alternative form of training that features a principled way to quantify uncertainty in model parameters. Bayes-GCNN would eliminate the need to run repetitive experiments with probabilistic representation of weights and biases. While the mean accuracy of the Bayes-GCNN was around 4-5% lower than canonical GCNN, the maximum accuracy is on par with the accuracy of canonical GCNN. In addition, canonical methods do not offer any uncertainty quantification which motivates implementation of Bayes-GCNN framework for real-world applications.

Code and Data

The code for Bayes-GCNN and data can be found on the Sydney Machine Learning Github repository ⁶.

References

- [1] F. Scarselli, M. Gori, A. C. Tsoi, M. Hagenbuchner, G. Monfardini, The graph neural network model, *IEEE Transactions on Neural Networks* 20 (1) (2008) 61–80.
- [2] Z. Wu, S. Pan, F. Chen, G. Long, C. Zhang, S. Y. Philip, A comprehensive survey on graph neural networks, *IEEE Transactions on Neural Networks and Learning Systems* (2020).
- [3] Z. Zhang, P. Cui, W. Zhu, Deep learning on graphs: A survey, *IEEE Transactions on Knowledge and Data Engineering* (2020).
- [4] K. Xu, W. Hu, J. Leskovec, S. Jegelka, How powerful are graph neural networks?, *arXiv preprint arXiv:1810.00826* (2018).
- [5] D. J. Cook, L. B. Holder, *Mining graph data*, John Wiley & Sons, 2006.
- [6] H. Gao, Z. Wang, S. Ji, Large-scale learnable graph convolutional networks, in: *Proceedings of the 24th ACM SIGKDD International Conference on Knowledge Discovery & Data Mining*, 2018, pp. 1416–1424.
- [7] F. Wu, T. Zhang, A. H. d. Souza Jr, C. Fifty, T. Yu, K. Q. Weinberger, Simplifying graph convolutional networks, *arXiv preprint arXiv:1902.07153* (2019).
- [8] M. Schlichtkrull, T. N. Kipf, P. Bloem, R. Van Den Berg, I. Titov, M. Welling, Modeling relational data with graph convolutional networks, in: *European Semantic Web Conference*, Springer, 2018, pp. 593–607.

⁶<https://github.com/sydney-machine-learning/BayesianGraphNeuralNetworks>

Table 5: Bayesian GCNN results comparison of established methods from literature. (Unavailable values are left blank.)

Method	Cora	CiteSeer	PubMed
	best (mean, std)	best (mean, std)	best (mean, std)
GCNN (SGD) [29] 2016	75.70 (,)	64.70 (,)	77.20 (,)
GCNN (Adam) [30] 2017	(81.50,)	(70.30,)	(79.00,)
GCNN* (SGD)	23.70 (16.78, 4.18)	25.60 (20.36, 2.74)	45.60 (38.13, 8.55)
Bayes-GCNN (SGD)	32.40 (15.42, 5.02)	25.20 (16.49, 2.78)	50.90 (37.75, 5.58)
GCNN* (Adam)	81.70 (80.81, 0.65)	72.00 (70.51, 0.85)	79.50 (79.00, 0.60)
Bayes-GCNN (Adam)	79.00 (74.71, 2.42)	68.90 (63.26, 2.74)	78.70 (74.94, 1.63)

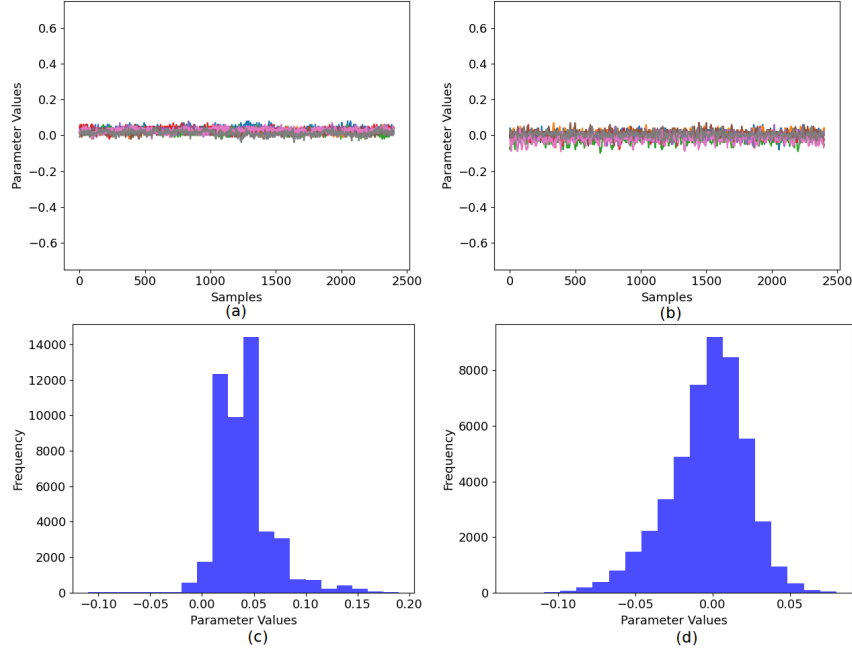


Figure 3: Posterior and trace plot for selected weights for Cora

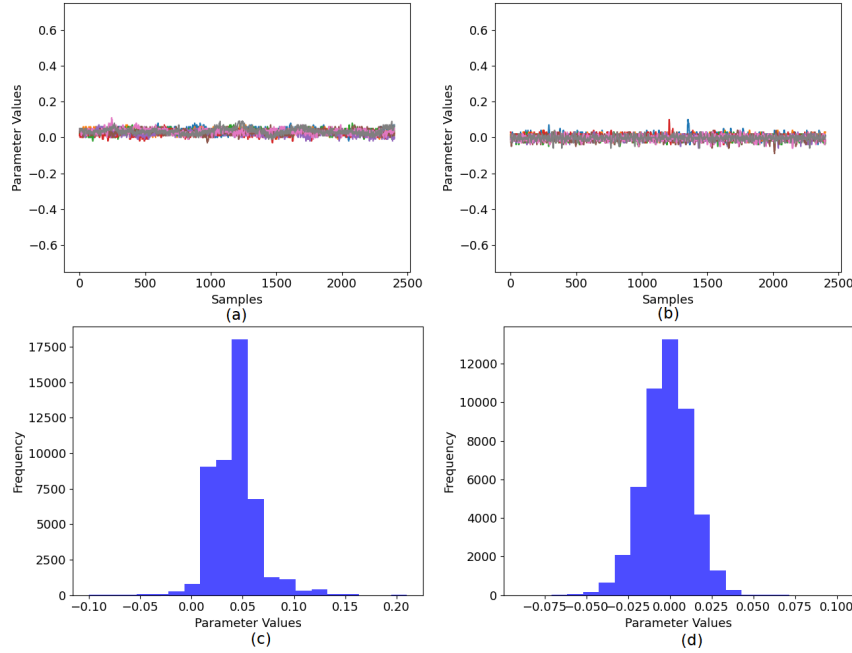


Figure 4: Posterior and trace plot for selected weights for CiteSeer

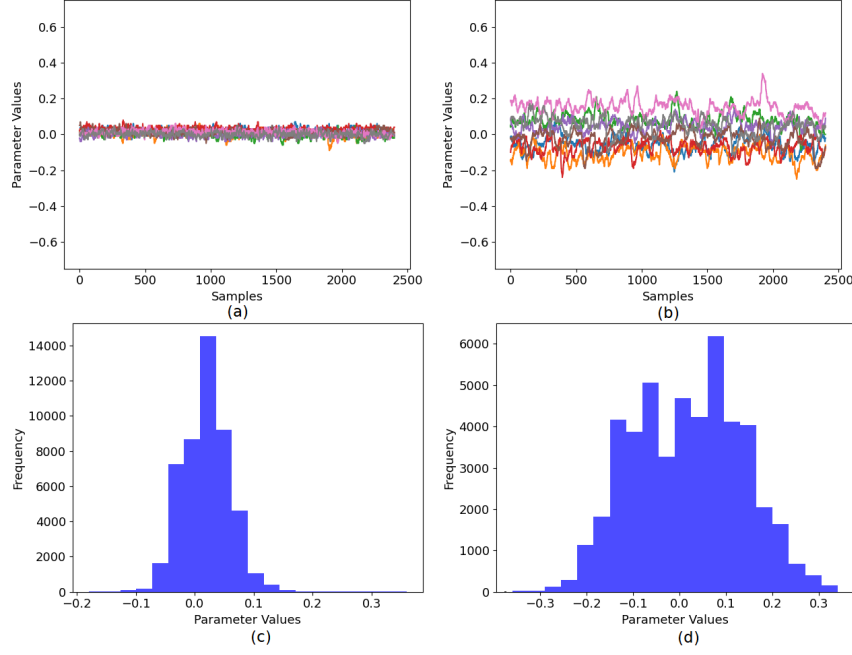


Figure 5: Posterior and trace plot for selected weights for PubMed

Table 6: Convergence diagnostics for the selected weights denoted by identity number (Weight-ID) for respective problems (Cora, CiteSeer, and PubMed)

Weight-ID	Cora	CiteSeer	PubMed
0	1.25	1.27	1.25
100	1.21	1.18	1.15
1000	1.15	1.16	1.23
5000	1.18	1.26	1.17
8000	1.22	1.28	1.20

[9] X. Liang, X. Shen, J. Feng, L. Lin, S. Yan, Semantic object parsing with graph lstm, in: European Conference on Computer Vision, Springer, 2016, pp. 125–143.

[10] V. Zayats, M. Ostendorf, Conversation modeling on reddit using a graph-structured lstm, Transactions of the Association for Computational Linguistics 6 (2018) 121–132.

[11] J. Tang, X. Shu, R. Yan, L. Zhang, Coherence constrained graph lstm for group activity recognition, IEEE transactions on pattern analysis and machine intelligence (2019).

[12] X. Shu, L. Zhang, Y. Sun, J. Tang, Host-parasite: Graph lstm-in-lstm for group activity recognition, IEEE Transactions on Neural Networks and Learning Systems (2020).

[13] C. Wang, S. Pan, G. Long, X. Zhu, J. Jiang, Mgae: Marginalized graph autoencoder for graph clustering, in: Proceedings of the 2017 ACM on Conference on Information and Knowledge Management, 2017, pp. 889–898.

[14] S. Pan, R. Hu, G. Long, J. Jiang, L. Yao, C. Zhang, Adversarially regularized graph autoencoder for graph embedding, arXiv preprint arXiv:1802.04407 (2018).

[15] H. Wang, J. Wang, J. Wang, M. Zhao, W. Zhang, F. Zhang, X. Xie, M. Guo, Graphgan: Graph representation learning with generative adversarial nets, arXiv preprint arXiv:1711.08267 (2017).

[16] Z. Wu, S. Pan, G. Long, J. Jiang, X. Chang, C. Zhang, Connecting the dots: Multivariate time series forecasting with graph neural networks, arXiv preprint arXiv:2005.11650 (2020).

[17] C. Chen, K. Li, S. G. Teo, X. Zou, K. Wang, J. Wang, Z. Zeng, Gated residual recurrent graph neural networks for traffic prediction, in: Proceedings of the AAAI Conference on Artificial Intelligence, Vol. 33, 2019, pp. 485–492.

[18] H. Peng, H. Wang, B. Du, M. Z. A. Bhuiyan, H. Ma, J. Liu, L. Wang, Z. Yang, L. Du, S. Wang, et al., Spatial temporal incidence dynamic graph neural networks for traffic flow forecasting, Information Sciences 521 (2020) 277–290.

[19] J. Shlomi, P. Battaglia, et al., Graph neural networks in particle physics, Machine Learning: Science and Technology (2020).

[20] O. Wieder, S. Kohlbacher, M. Kuenemann, A. Garon, P. Ducrot, T. Seidel, T. Langer, A compact review of molecular property prediction with graph neural networks, Drug Discovery Today: Technologies (2020).

[21] M. Wang, G. Hu, A novel method for twitter sentiment analysis based on attentional-graph neural network, Information 11 (2) (2020) 92.

[22] H. Wang, F. Zhang, M. Zhang, J. Leskovec, M. Zhao, W. Li, Z. Wang, Knowledge-aware graph neural networks with label smoothness regularization for recommender systems, in: Proceedings of the 25th ACM SIGKDD International Conference on Knowledge Discovery & Data Mining, 2019, pp. 968–977.

[23] Q. Cao, H. Shen, J. Gao, B. Wei, X. Cheng, Popularity prediction on social platforms with coupled graph neural networks, in: Proceedings of the 13th International Conference on Web Search and Data Mining, 2020, pp. 70–78.

[24] J. Zhou, G. Cui, Z. Zhang, C. Yang, Z. Liu, L. Wang, C. Li, M. Sun, Graph neural networks: A review of methods and applications, arXiv preprint arXiv:1812.08434 (2018).

[25] Y. Lecun, L. Bottou, Y. Bengio, P. Haffner, Gradient-based learning applied to document recognition, Proceedings of the IEEE 86 (11) (1998) 2278–2324.

[26] O. Russakovsky, J. Deng, H. Su, J. Krause, S. Satheesh, S. Ma, Z. Huang, A. Karpathy, A. Khosla, M. Bernstein, Imagenet large scale visual recognition challenge, Int. J. Conflict Violence (IJCV) 115 (3) (2015) 211–252.

[27] S. Hochreiter, J. Schmidhuber, Long short-term memory, Neural computation 9 (8) (1997) 1735–1780.

[28] J. Schmidhuber, Deep learning in neural networks: An overview, Neural networks 61 (2015) 85–117.

[29] Z. Yang, W. W. Cohen, R. Salakhutdinov, Revisiting semi-supervised learning with graph embeddings, CoRR abs/1603.08861 (2016). arXiv: 1603.08861. URL <http://arxiv.org/abs/1603.08861>

[30] T. N. Kipf, M. Welling, Semi-supervised classification with graph convolutional networks, CoRR abs/1609.02907 (2016). arXiv: 1609.02907. URL <http://arxiv.org/abs/1609.02907>

[31] R. M. Neal, Sampling from multimodal distributions using tempered tran-

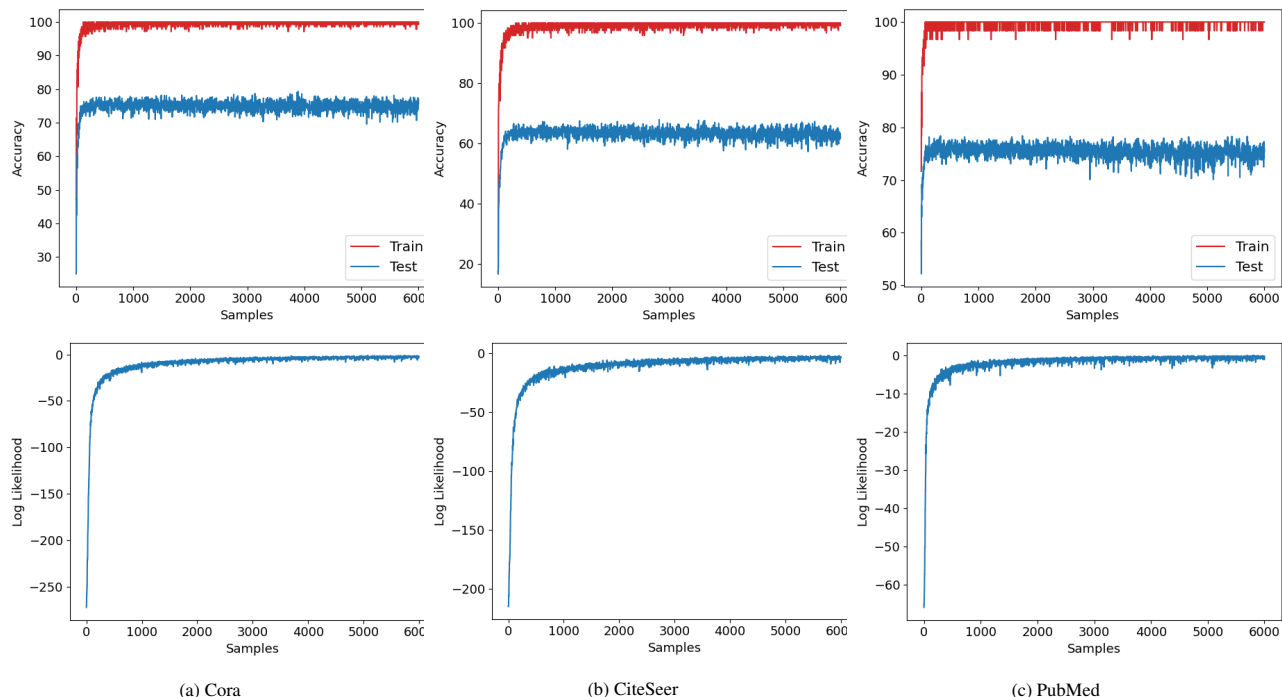


Figure 6: Accuracy And Log-Likelihood for different problems

- sitions, *Statistics and computing* 6 (4) (1996) 353–366.
- [32] M. Welling, Y. W. Teh, Bayesian learning via stochastic gradient langevin dynamics, in: *Proceedings of the 28th International Conference on Machine Learning (ICML-11)*, 2011, pp. 681–688.
- [33] R. Chandra, K. Jain, A. Kapoor, A. Aman, Surrogate-assisted parallel tempering for bayesian neural learning, *Engineering Applications of Artificial Intelligence* 94 (2020) 103700.
- [34] R. Chandra, K. Jain, R. V. Deo, S. Cripps, Langevin-gradient parallel tempering for bayesian neural learning, *Neurocomputing* 359 (2019) 315–326.
- [35] C. Blundell, J. Cornebise, K. Kavukcuoglu, D. Wierstra, Weight uncertainty in neural network, in: *Proceedings of The 32nd International Conference on Machine Learning*, 2015, pp. 1613–1622.
- [36] R. Chandra, K. Jain, R. V. Deo, S. Cripps, Langevin-gradient parallel tempering for bayesian neural learning, *Neurocomputing* 359 (2019) 315–326.
- [37] J. A. Bondy, U. S. R. Murty, et al., *Graph theory with applications*, Vol. 290, Macmillan London, 1976.
- [38] D. B. West, et al., *Introduction to graph theory*, Vol. 2, Prentice hall Upper Saddle River, 2001.
- [39] J. Gilmer, S. S. Schoenholz, P. F. Riley, O. Vinyals, G. E. Dahl, Neural message passing for quantum chemistry, *CoRR abs/1704.01212* (2017). [arXiv:1704.01212](https://arxiv.org/abs/1704.01212). URL <http://arxiv.org/abs/1704.01212>
- [40] P. Veličković, G. Cucurull, A. Casanova, A. Romero, P. Liò, Y. Bengio, Graph attention networks (2018). [arXiv:1710.10903](https://arxiv.org/abs/1710.10903).
- [41] J. Zhang, X. Shi, J. Xie, H. Ma, I. King, D. Yeung, Gaan: Gated attention networks for learning on large and spatiotemporal graphs, *CoRR abs/1803.07294* (2018). [arXiv:1803.07294](https://arxiv.org/abs/1803.07294). URL <http://arxiv.org/abs/1803.07294>
- [42] Y. Li, D. Tarlow, M. Brockschmidt, R. Zemel, Gated graph sequence neural networks (2017). [arXiv:1511.05493](https://arxiv.org/abs/1511.05493).
- [43] V. Zayats, M. Ostendorf, Conversation modeling on reddit using a graph-structured lstm, *Transactions of the Association for Computational Linguistics* 6 (2018) 121–132. [arXiv:https://doi.org/10.1162/tac1_a_00009](https://doi.org/10.1162/tac1_a_00009), doi:10.1162/tac1_a_00009. URL https://doi.org/10.1162/tac1_a_00009
- [44] A. Rahimi, T. Cohn, T. Baldwin, Semi-supervised user geolocation via graph convolutional networks, in: *Proceedings of the 56th Annual Meeting of the Association for Computational Linguistics (Volume 1: Long Papers)*, Association for Computational Linguistics, Melbourne, Australia, 2018, pp. 2009–2019. doi:10.18653/v1/P18-1187. URL <https://www.aclweb.org/anthology/P18-1187>
- [45] K. Xu, C. Li, Y. Tian, T. Sonobe, K. Kawarabayashi, S. Jegelka, Representation learning on graphs with jumping knowledge networks, *CoRR abs/1806.03536* (2018). [arXiv:1806.03536](https://arxiv.org/abs/1806.03536). URL <http://arxiv.org/abs/1806.03536>
- [46] M. Simonovsky, N. Komodakis, Dynamic edge-conditioned filters in convolutional neural networks on graphs, *CoRR abs/1704.02901* (2017). [arXiv:1704.02901](https://arxiv.org/abs/1704.02901). URL <http://arxiv.org/abs/1704.02901>
- [47] J. Atwood, D. Towsley, Diffusion-convolutional neural networks, *CoRR abs/1511.02136* (2015). [arXiv:1511.02136](https://arxiv.org/abs/1511.02136). URL <http://arxiv.org/abs/1511.02136>
- [48] D. Duvenaud, D. Maclaurin, J. Aguilera-Iparraguirre, R. Gómez-Bombarelli, T. Hirzel, A. Aspuru-Guzik, R. P. Adams, Convolutional networks on graphs for learning molecular fingerprints, *CoRR abs/1509.09292* (2015). [arXiv:1509.09292](https://arxiv.org/abs/1509.09292). URL <http://arxiv.org/abs/1509.09292>
- [49] C. Zhuang, Q. Ma, Dual graph convolutional networks for graph-based semi-supervised classification, in: *Proceedings of the 2018 World Wide Web Conference, WWW '18, International World Wide Web Conferences Steering Committee, Republic and Canton of Geneva, CHE*, 2018, p. 499–508. doi:10.1145/3178876.3186116. URL <https://doi.org/10.1145/3178876.3186116>
- [50] F. Monti, D. Boscaini, J. Masci, E. Rodolà, J. Svoboda, M. M. Bronstein, Geometric deep learning on graphs and manifolds using mixture model cnns, *CoRR abs/1611.08402* (2016). [arXiv:1611.08402](https://arxiv.org/abs/1611.08402). URL <http://arxiv.org/abs/1611.08402>
- [51] D. K. Hammond, P. Vandergheynst, R. Gribonval, Wavelets on graphs via spectral graph theory, *Applied and Computational Harmonic Analysis* 30 (2) (2011) 129–150. doi:https://doi.org/10.1016/j.acha.2010.04.005. URL <https://www.sciencedirect.com/science/article/pii/S1063520310000552>
- [52] R. Li, S. Wang, F. Zhu, J. Huang, Adaptive graph convolutional neural networks, *CoRR abs/1801.03226* (2018). [arXiv:1801.03226](https://arxiv.org/abs/1801.03226). URL <http://arxiv.org/abs/1801.03226>

- [53] W. L. Hamilton, R. Ying, J. Leskovec, Inductive representation learning on large graphs, CoRR abs/1706.02216 (2017). arXiv:1706.02216. URL <http://arxiv.org/abs/1706.02216>
- [54] R. Ying, R. He, K. Chen, P. Eksombatchai, W. L. Hamilton, J. Leskovec, Graph convolutional neural networks for web-scale recommender systems, CoRR abs/1806.01973 (2018). arXiv:1806.01973. URL <http://arxiv.org/abs/1806.01973>
- [55] J. Chen, T. Ma, C. Xiao, Fastgcn: Fast learning with graph convolutional networks via importance sampling, CoRR abs/1801.10247 (2018). arXiv:1801.10247. URL <http://arxiv.org/abs/1801.10247>
- [56] J. Chen, J. Zhu, L. Song, Stochastic training of graph convolutional networks with variance reduction (2018). arXiv:1710.10568.
- [57] H. Gao, Z. Wang, S. Ji, Large-scale learnable graph convolutional networks, CoRR abs/1808.03965 (2018). arXiv:1808.03965. URL <http://arxiv.org/abs/1808.03965>
- [58] T. N. Kipf, M. Welling, Variational graph auto-encoders, arXiv preprint arXiv:1611.07308 (2016).
- [59] S. Pan, R. Hu, G. Long, J. Jiang, L. Yao, C. Zhang, Adversarially regularized graph autoencoder for graph embedding (2019). arXiv:1802.04407.
- [60] H. Wang, D.-Y. Yeung, A survey on bayesian deep learning, ACM Computing Surveys (CSUR) 53 (5) (2020) 1–37.
- [61] N. G. Polson, V. Sokolov, et al., Deep learning: A bayesian perspective, Bayesian Analysis 12 (4) (2017) 1275–1304.
- [62] M. J. Kusner, B. Paige, J. M. Hernández-Lobato, Grammar variational autoencoder, in: International Conference on Machine Learning, PMLR, 2017, pp. 1945–1954.
- [63] L. Mescheder, S. Nowozin, A. Geiger, Adversarial variational bayes: Unifying variational autoencoders and generative adversarial networks, in: International Conference on Machine Learning, PMLR, 2017, pp. 2391–2400.
- [64] C. Zhao, B. Ni, J. Zhang, Q. Zhao, W. Zhang, Q. Tian, Variational convolutional neural network pruning, in: Proceedings of the IEEE/CVF Conference on Computer Vision and Pattern Recognition, 2019, pp. 2780–2789.
- [65] J.-T. Chien, K.-T. Kuo, et al., Variational recurrent neural networks for speech separation, in: 18TH ANNUAL CONFERENCE OF THE INTERNATIONAL SPEECH COMMUNICATION ASSOCIATION (INTERSPEECH 2017), VOLS 1-6: SITUATED INTERACTION, 2017, pp. 1193–1197.
- [66] X. Zhou, Y. Hu, W. Liang, J. Ma, Q. Jin, Variational lstm enhanced anomaly detection for industrial big data, IEEE Transactions on Industrial Informatics (2020).
- [67] J. Su, S. Wu, D. Xiong, Y. Lu, X. Han, B. Zhang, Variational recurrent neural machine translation, CoRR abs/1801.05119 (2018). arXiv:1801.05119. URL <http://arxiv.org/abs/1801.05119>
- [68] S. Bonner, A. Atapour-Abarghouei, P. T. Jackson, J. Brennan, I. Kureshi, G. Theodoropoulos, A. S. McGough, B. Obara, Temporal neighbourhood aggregation: Predicting future links in temporal graphs via recurrent variational graph convolutions, in: 2019 IEEE International Conference on Big Data (Big Data), IEEE, 2019, pp. 5336–5345.
- [69] M. Qu, Y. Bengio, J. Tang, Gmn: Graph markov neural networks, in: International conference on machine learning, PMLR, 2019, pp. 5241–5250.
- [70] Y. Gal, Z. Ghahramani, Bayesian convolutional neural networks with bernoulli approximate variational inference, arXiv preprint arXiv:1506.02158 (2015).
- [71] R. M. Neal, et al., Mcmc using hamiltonian dynamics, Handbook of Markov Chain Monte Carlo 2 (11) (2011).
- [72] D. Levy, M. D. Hoffman, J. Sohl-Dickstein, Generalizing Hamiltonian Monte Carlo with neural networks, arXiv preprint arXiv:1711.09268 (2017).
- [73] A. D. Cobb, B. Jalaian, Scaling Hamiltonian Monte Carlo inference for bayesian neural networks with symmetric splitting, arXiv preprint arXiv:2010.06772 (2020).
- [74] R. Chandra, K. Jain, A. Kapoor, A. Aman, Surrogate-assisted parallel tempering for bayesian neural learning, Engineering Applications of Artificial Intelligence 94 (2020) 103700.
- [75] R. Chandra, A. Kapoor, Bayesian neural multi-source transfer learning, Neurocomputing 378 (2020) 54–64.
- [76] D. P. Kingma, J. Ba, Adam: A method for stochastic optimization, arXiv preprint arXiv:1412.6980 (2014).
- [77] R. H. Swendsen, J.-S. Wang, Replica monte carlo simulation of spin-glasses, Physical review letters 57 (21) (1986) 2607.
- [78] K. Hukushima, K. Nemoto, Exchange monte carlo method and application to spin glass simulations, Journal of the Physical Society of Japan 65 (6) (1996) 1604–1608.
- [79] U. H. Hansmann, Parallel tempering algorithm for conformational studies of biological molecules, Chemical Physics Letters 281 (1-3) (1997) 140–150.
- [80] M. K. Sen, P. L. Stoffa, Bayesian inference, gibbs’ sampler and uncertainty estimation in geophysical inversion, Geophysical Prospecting 44 (2) (1996) 313–350.
- [81] M. Maraschini, S. Foti, A monte carlo multimodal inversion of surface waves, Geophysical Journal International 182 (3) (2010) 1557–1566.
- [82] R. Chandra, R. D. Müller, D. Azam, R. Deo, N. Butterworth, T. Salles, S. Cripps, Multicore parallel tempering Bayeslands for basin and landscape evolution, Geochemistry, Geophysics, Geosystems 20 (11) (2019) 5082–5104.
- [83] P. Sen, G. Namata, M. Bilgic, L. Getoor, B. Galligher, T. Eliassi-Rad, Collective classification in network data, AI magazine 29 (3) (2008) 93–93.
- [84] Q. Lu, L. Getoor, Link-based classification, in: T. Fawcett, N. Mishra (Eds.), Machine Learning, Proceedings of the Twentieth International Conference (ICML 2003), August 21–24, 2003, Washington, DC, USA, AAAI Press, 2003, pp. 496–503. URL <http://www.aaai.org/Library/ICML/2003/icml03-066.php>
- [85] G. Namata, B. London, L. Getoor, B. Huang, Query-driven active surveying for collective classification, in: ICML Workshop on MLG, 2012, p. 789.
- [86] D. Vats, C. Knudson, Revisiting the gelman-rubin diagnostic (2020). arXiv:1812.09384.
- [87] G. O. Roberts, J. S. Rosenthal, Coupling and ergodicity of adaptive markov chain monte carlo algorithms, Journal of Applied Probability 44 (2) (2007) 458–475. doi:10.1239/jap/1183667414.
- [88] J. M. Flegal, M. Haran, G. L. Jones, Markov chain monte carlo: Can we trust the third significant figure?, Statistical Science 23 (2) (2008) 250–260. doi:10.1214/08-sts257. URL <http://dx.doi.org/10.1214/08-STs257>
- [89] V. Roy, Convergence diagnostics for markov chain monte carlo (2019). arXiv:1909.11827.
- [90] M. K. Cowles, B. P. Carlin, Markov chain monte carlo convergence diagnostics: A comparative review, Journal of the American Statistical Association 91 (434) (1996) 883–904. arXiv:https://www.tandfonline.com/doi/pdf/10.1080/01621459.1996.10476956, doi:10.1080/01621459.1996.10476956. URL <https://www.tandfonline.com/doi/abs/10.1080/01621459.1996.10476956>
- [91] T. Bogaerts, A. D. Masegosa, J. S. Angarita-Zapata, E. Onieva, P. Hellinckx, A graph cnn-lstm neural network for short and long-term traffic forecasting based on trajectory data, Transportation Research Part C: Emerging Technologies 112 (2020) 62–77. doi:https://doi.org/10.1016/j.trc.2020.01.010. URL <https://www.sciencedirect.com/science/article/pii/S0968090X19309349>
- [92] Y. Yin, X. Zheng, B. Hu, Y. Zhang, X. Cui, Eeg emotion recognition using fusion model of graph convolutional neural networks and lstm, Applied Soft Computing 100 (2021) 106954. doi:https://doi.org/10.1016/j.asoc.2020.106954. URL <http://www.sciencedirect.com/science/article/pii/S1568494620308929>
- [93] B. Donon, R. Clément, B. Donnot, A. Marot, I. Guyon, M. Schoenauer, Neural networks for power flow: Graph neural solver, Electric Power Systems Research 189 (2020) 106547. doi:https://doi.org/10.1016/j.epsr.2020.106547. URL <http://www.sciencedirect.com/science/article/pii/S0378779620303515>
- [94] R. Ramakrishnan, P. O. Dral, M. Rupp, O. A. von Lilienfeld, Quantum chemistry structures and properties of 134 kilo molecules, Scientific Data

- 1 (2014).
- [95] L. Ruddigkeit, R. van Deursen, L. C. Blum, J.-L. Reymond, Enumeration of 166 billion organic small molecules in the chemical universe database gdb-17, *Journal of Chemical Information and Modeling* 52 (11) (2012) 2864–2875, pMID: 23088335. *arXiv*:<https://doi.org/10.1021/ci300415d>, doi:10.1021/ci300415d. URL <https://doi.org/10.1021/ci300415d>
 - [96] K. Borgwardt, C. ONG, S. Schönauer, S. Vishwanathan, A. Smola, H. Kriegel, Protein function prediction via graph kernels, *Bioinformatics* 21 Suppl 1 (2005) i47–56.
 - [97] I. Schomburg, A. Chang, C. Ebeling, M. Gremse, C. Heldt, G. Huhn, D. Schomburg, Brenda, the enzyme database: Updates and major new developments, *Nucleic acids research* 32 (2004) D431–3. doi:10.1093/nar/gkh081.
 - [98] P. Yanardag, S. Vishwanathan, Deep graph kernels, in: *Proceedings of the 21th ACM SIGKDD International Conference on Knowledge Discovery and Data Mining, KDD '15*, Association for Computing Machinery, New York, NY, USA, 2015, p. 1365–1374. doi:10.1145/2783258.2783417. URL <https://doi.org/10.1145/2783258.2783417>
 - [99] M. Betancourt, A conceptual introduction to hamiltonian monte carlo (2018). *arXiv*:1701.02434.